EUROPEAN ORGANIZATION FOR NUCLEAR RESEARCH

CERN/TIS-RP/97-09/CF

Radiation calculations for the new muon/photon test facility at CERN

S. Agosteo[1] and M. Silari[2]

[1] Politecnico di Milano, CESNEF, Via Ponzio 34/3, 20133 Milan, Italy
[2] CERN, 1211 Geneva 23, Switzerland

Abstract

A new irradiation facility has recently been set up in the West Experimental Area at CERN. It consists of a 740 GBq (20 Ci) ^{137}Cs source combined with a high energy muon beam. The facility will be used to test detectors for the future Large Hadron Collider (LHC) experimental apparatus in the presence of an intense photon flux, to simulate the expected background during operation of the LHC. Irradiation positions are available for testing of both small components and large chambers. The possibility of varying the photon flux in a controlled way is provided by a set of mobile lead filters. Monte Carlo simulations with the MCNP code were performed to evaluate the influence of the filters and of wall and floor scattering on the photon spectrum at the irradiation points, as well as to estimate the dose equivalent at the access doors to the zone.

Presented at the Third Workshop on
Simulation of Accelerator Radiation Environments (SARE3)
KEK, Tsukuba, Japan, 7-9 May, 1997

CERN, 1211 Geneva 23, Switzerland
15 April 1997

1. Introduction

A new irradiation facility has been set up at CERN, downstream of the final dump of the X5 beam, one of the secondary beam lines of the West Experimental Area (WA) of the Super Proton Synchrotron (SPS). This zone, shown in Fig. 1, has been equipped with a 740 GBq (20 Ci) ^{137}Cs source which will be used to irradiate, in two different positions, large detectors (with dimensions up to 6 m x 3 m) developed for the future experiments at the LHC. The aim is to irradiate the detectors with a low muon flux (10^4 muons per SPS pulse) from the X5 beam and measure the effect of the photon background (which reproduces the background expected during operation of the LHC) on the detector efficiency and resolution. The strenght of the ^{137}Cs source was chosen according to the requirement of a photon flux at the detector position in the range 10^3 to $2x10^4$ s^{-1} cm^{-2}, taking into account that the sensitivity of the detectors to the 662 keV photons is 3 to 5%. The variation of the flux will be achieved by a set of (adjustable) lead filters, remotely controlled, installed in front of the source.

While the large detectors will be irradiated in the forward direction by a combined muon/photon flux, a second test position is provided at 90° with respect to the X5 beam line, at 0.6 m from the source, to allow irradiation of small crystals (with maximum transverse dimensions of 20x20 cm^2) in a "parasitic" mode, i.e. without interfering with the test of the large chambers.

The safety aspects of this new installation, called Gamma Irradiation Facility (GIF), are dictated by the operation of the source (producing a dose rate of about 60 mSv/h at 1 m), the muon flux being too weak to pose any hazard. A search procedure of the area will be required before the zone can be locked; the same (and unique) key which gives access to the zone must be inserted in the console controlling operation of the source, so that the source can leave its shielded position only if the area is cleared and locked up. The operation of the source can (and will) be interlocked to the operation of the beam line if in the future other particles than muons (e.g., electrons) will be used. The source (including shielding) was bought from and installed by a specialised firm, which also provided the safety system and the radiation monitors, subsequently interfaced to the CERN control system. The source assembly is thoroughly described in the next section.

The irradiation area is surrounded by concrete shielding 8.4 m high and 80 cm thick, but with no roof. Access will normally be through a standard Personal Protection Entry (PPE) door. The safety exit (PPX) door will also be used to take the small components irradiated in the lateral position outside the GIF area, into an adjacent test area, which is accessible while the source is operating. The large chambers will be introduced into the zone through a gate close to the PPE door.

The GIF will be used by various groups (mainly from the ATLAS and CMS collaborations), but there will be only one main user at a time, who will be responsible for the source operation. The irradiation area can in principle be modified according to the user's requirement. The source is installed at about 3 m above floor level of the WA, 60 cm below the X5 beam line and slightly off-centre with respect to the muon beam. Three slightly different configurations of the GIF floor have been foreseen, according to the requests made by the various users. In the original design, the floor level in the GIF is the same as that of the WA (we will call it case 1). For the irradiation of the small crystals a concrete platform at 2.4 m above the floor was introduced around the source, for easy transportation of the crystal and

its cryostat out of the irradiation area via the PPX door (case 2, shown in Fig. 1). A third possibility is to extend the platform to the entire zone, except for a limited area in the proximity of the access gate and of the PPE door (case 3). In this case the source is only 61 cm above the platform. This configuration will be used for testing smaller chambers.

The detector tests require in principle monoenergetic photons, so that a careful assessment of the modification of the source emission produced by the lead filters and by wall and floor scattering is important. Monte Carlo simulations of the complete facility were carried out with the MCNP code to evaluate the photon spectrum in the forward irradiation position closer to the end wall, as well as for the lateral position. The dose rate expected at the gate and at the PPX door, which are not shielded, was also calculated.

2. Simulations

The simulations were performed with the MCNP-4A code [1] in the photon-electron mode. The transport of electrons was cut off at 100 keV, to save CPU time cutting out a large number of secondaries whose contribution is of no interest for the present work. However, the production of bremsstrahlung and fluorescence x- rays was taken into account, except for the 32.2 keV fluorescence x-rays following the internal conversion of ^{137m}Ba, which were neglected. The present simulations were completely analogue, i.e. no variance reduction techniques were used.

The SABRINA graphic package [2] was used to draw the 3D views of the MCNP input file geometry. Fig. 2 shows a 3D sectional view of the ^{137}Cs source capsule. The source core material is cesium sulfate, embedded in glass, while the encapsulation is in welded stainless steel AISI 316 (external dimensions: diameter 12.45 mm, height 17.7 mm). The spatial and angular distributions of the photon source were considered uniform (in the cesium sulfate core) and isotropic, respectively. The emitted photons are monoenergetic (661.6 keV).

The source is placed inside a cylindrical shielding assembly (diameter 260 mm, height 435 mm) with walls of stainless steel AISI 316, 7 mm thick, filled with lead. Two radial conic apertures (collimators), subtending polar angles of 37° and 10° (Fig. 3), open in the forward (parallel to the X5 beam line) and lateral (at 90° to the beam line) directions. A lead filter is placed in front of the forward aperture at 144 mm from the source centre. The effect of 20 mm and 40 mm filters was investigated. The lateral aperture is not filtered.

The shielding assembly is in turn enclosed in an AISI 316 box (Fig. 3) with walls 28.6 mm thick. Two conic guides in lead (thickness 14.3 mm) are located in the air gap between the source shield and the box wall, adjacent to the apertures described above.

In the first configuration considered (case 1), the source assembly is placed at the top of a concrete block, 2.4 m above the floor (Fig. 4). Concrete walls (4.8 m high, 0.8 m thick) are placed around the source, to shield it locally in the lateral and backward directions. The irradiation area is surrounded by concrete walls 8.4 m high and 0.8 m thick. A 3D sectional view of the facility is shown in Fig. 5. All the cells not in solid materials were filled with air.

The photon current (i.e. the number of photons crossing a surface) was scored in the forward and lateral directions at 4 m and at 60 cm from the source, respectively. These distances

correspond to the irradiation positions of the detectors to be tested in the photon/muon field. The scoring surfaces were subdivided in concentric rings, in order to obtain an angular binning of the impinging photons. The photon current was also scored in energy bins, highly discretised in the energy range 1-100 keV, to emphasise the presence of fluorescence x-rays (mainly from Pb at about 75 keV). A very narrow energy group was considered for scoring the uncollided 661.2 keV photons, in order to sharply separate them from the scattered component of the spectrum.

A second series of simulations was performed for the case 2 described above (Fig. 6). The platform material was also concrete. In this configuration, one of the lateral walls in proximity of the source was removed and part of the back wall was thinned down to 40 cm. In this configuration, the access gate to the irradiation area and the PPX door at the back side of the platform were taken into account. The photon spectra were scored at the same irradiation positions as above. The forward Pb filter was 2 cm thick. The scoring geometry was the same as in the configuration without platform. It should be noticed that in every angular bin, some photons can interact with the platform edge. This effect is more remarkable at the larger scoring angular bins.

A third configuration with the 2.4 m high platform extended to the whole facility was also considered (case 3, shown in Fig. 7). Forward scoring was performed only in the upper part of the annular rings not intersecting the concrete floor. The filter thickness was 2 cm.

Finally, the dose equivalent per source photon was calculated at the access gate and at the PPX door for cases 2 and 3. The fluence to dose equivalent conversion factors were taken from ref. [3].

3. Results and discussion

The current density, i.e. the number of photons crossing each scoring ring normalised to the ring area, calculated in the forward and lateral directions are listed in Table 1 for case 1. The data for the forward direction are given separately for the 2 cm and 4 cm lead filters.

The scattered component is obviously lower in the lateral direction, both because the scoring area is closer to the source and because the radiation is not filtered. The ratio of the direct to the scattered component remains approximately constant within the investigated angular range, being about 5 at 0°-2° and about 4 at 8°-10°. The direct current density decreases with increasing angle. This may be explained by the combined effect of self-attenuation in the source and of the increase with angle of the distance between source and scoring position. At large scoring angles, photons cover a longer path through the cesium sulfate core and the stainless steel encapsulation, thus undergoing a larger interaction probability. Moreover, as the scoring rings lay on a plane, an inverse square distance effect should be considered with increasing scoring angle: for a point source the current density at 10° should be about 3% lower than that at 0°. A smoother decrease obviously characterises the scattered component.

The effect of the side wall (behind the lateral scoring area) is negligible. Fig. 8 shows the energy distribution of the current density in the lateral direction. The shape of the energy distribution is independent of the scoring angle. The peak at about 75 keV is due to the fluorescence x rays of lead.

distribution is independent of the scoring angle. The peak at about 75 keV is due to the fluorescence x rays of lead.

Fig. 9 shows the energy distribution of the current density at the forward irradiation position with the 2 cm lead filter. Both direct and scattered component decrease with scoring angle (see Table 1). It should be noted that in this case the influence of the inverse square distance effect is larger, reducing the current density by about 57% from 0° to 37° (for a point source). The self-attenuation effect is larger because of the 2 cm filter and further increases with the 4 cm filter (see Table 1).

Figs. 10-16 show the energy distributions, at each scoring angle, of the current density in the forward irradiation position with 2 cm and 4 cm filters. It should be noted that the attenuation of both components increases with the scoring angle (see also Table 1).

Figs. 17-18 show the energy distribution of the current density in the forward irradiation position for cases 2 and 3 (partial platform and full platform). The values of current density are listed in Tables 2 and 3.

The current density in the lateral position does not vary much with or without platform and lateral wall. It should be noted that the data for the lateral direction in Tables 2 and 3 are the same, thus stressing that the extension of the platform has no influence in this irradiation position. The values are identical because the random seed and the number of histories used in the simulations were the same, to emphasise the eventual perturbations with respect to the unmodified part of the geometry.

The current density in the forward position remains almost constant up to 15° for cases 2 and 3. At larger angles the attenuation of the direct and the scattered components is evident for case 2, because of the interactions with the platform edge. The direct component at the forward position for cases 1 and 3 (see Tables 1 and 3) is obviously unchanged, while the scattered one slightly increases for case 3.

Finally, Table 4 lists the dose equivalent per source photon and the dose rate calculated for a 740 GBq (20 Ci) source at the access gate and at the PPX door for cases 2 and 3. The largest value (7.15×10^{-22} Sv per photon) is found at the PPX door for case 3.

4. Conclusions

The following conclusions can be drawn for the three geometrical configurations and the two lead filters examined for the GIF. Cases 1 and 3, i.e. source placed at 3.6 m above the floor (no platform) and at 1.2 m above the floor (full platform), respectively, represent the two extreme conditions in terms of contribution from scattered radiation to the photon spectum at the test positions.

For the lateral irradiation position, the results are quite similar for the three cases, because of the proximity of the source, of the small collimation and of the absence of filtration. The results are not much influenced by the presence (or not) of the side shielding wall. The number of photons per cm^2 at the centre of the irradiation position (0.6 m from the source) are about 10^{-5} per source photon emitted isotropically by the source (i.e., about 5×10^6

photons s^{-1} cm^{-2} for the 20 Ci source), and about half this value at the edge of the solid angle defined by the collimators; about 80% are uncollided (E=662 keV), the rest being degraded into a broad energy distribution.

In the forward irradiation position, the photon flux decreases by about a factor 10 with the 2 cm lead filter, and by an additional factor 10 with the 4 cm filter. For the three geometrical configuration considered, approximately 50% of the original photons emitted in the solid angle defined by the collimation system are uncollided. The scattered component slighlty increases (by about 15%) from case 1 to case 3. With the 2 cm filter, the number of 662 keV photons per cm^2 at the centre of the irradiation area (4 m from the source) are about 3.5×10^{-8} per source photon emitted isotropically by the source (i.e., about 2.5×10^4 photons s^{-1} cm^{-2} for the 20 Ci source). At the edge of the solid angle defined by the collimator this value reduces to about 8.4×10^3, 5.3×10^3 and 8.7×10^3 photons s^{-1} cm^{-2} for cases 1, 2 and 3, respectively.

Dose rates in accessible areas (just outside the access gate and the PPE and PPX doors, which are unshielded) are at maximum 2 μSv/h.

Acknowledgements

We wish to thank A. Bonifas (CERN), responsible for the source installation, for useful discussions.

References

[1] J.F. Briestmeister, Ed., MCNP - A General Monte Carlo N-Particle Transport Code, Los Alamos National Laboratories LA-12625-M, Los Alamos, New Mexico, 1993.

[2] K.A. Van Riper, SABRINA User's Guide, Los Alamos National Laboratories LA-UR-93-3696, Los Alamos, New Mexico, 1994.

[3] ICRP Committee 3 Task Group, P. Grande and M.C. O'Riordan, Chairmen, Data for Protection against Ionizing Radiation from External Sources: Supplement to ICRP Publication 15, ICRP-21, International Commission on Radiological Protection, Pergamon Press, 1971.

TABLES

Table 1 - Current density (cm^{-2}) per source photon at the forward and lateral irradiation positions for the configuration without platform (case 1).

	Lateral			
	Scattered component (E < 661.6 keV)		Direct component (E = 661.6 keV)	
0°-2°	$(1.897\pm0.067)\cdot10^{-6}$		$(9.450\pm0.149)\cdot10^{-6}$	
2°-4°	$(1.923\pm0.039)\cdot10^{-6}$		$(9.139\pm0.085)\cdot10^{-6}$	
4°-6°	$(1.843\pm0.029)\cdot10^{-6}$		$(8.242\pm0.062)\cdot10^{-6}$	
6°-8°	$(1.640\pm0.023)\cdot10^{-6}$		$(7.141\pm0.049)\cdot10^{-6}$	
8°-10°	$(1.507\pm0.019)\cdot10^{-6}$		$(5.826\pm0.038)\cdot10^{-6}$	
	Forward			
	Pb filter 2 cm		Pb filter 4 cm	
	Scattered component (E < 661.6 keV)	Direct component (E = 661.6 keV)	Scattered component (E < 661.6 keV)	Direct component (E = 661.6 keV)
0°-5°	$(3.179\pm0.064)\cdot10^{-8}$	$(3.684\pm0.069)\cdot10^{-8}$	$(4.752\pm0.200)\cdot10^{-9}$	$(3.670\pm0.176)\cdot10^{-9}$
5°-10°	$(3.102\pm0.036)\cdot10^{-8}$	$(3.509\pm0.039)\cdot10^{-8}$	$(4.595\pm0.113)\cdot10^{-9}$	$(3.267\pm0.095)\cdot10^{-9}$
10°-15°	$(2.845\pm0.026)\cdot10^{-8}$	$(3.195\pm0.028)\cdot10^{-8}$	$(4.069\pm0.080)\cdot10^{-9}$	$(2.953\pm0.068)\cdot10^{-9}$
15°-20°	$(2.522\pm0.020)\cdot10^{-8}$	$(2.802\pm0.022)\cdot10^{-8}$	$(3.434\pm0.061)\cdot10^{-9}$	$(2.547\pm0.052)\cdot10^{-9}$
20°-25°	$(2.159\pm0.016)\cdot10^{-8}$	$(2.384\pm0.017)\cdot10^{-8}$	$(2.954\pm0.048)\cdot10^{-9}$	$(1.908\pm0.038)\cdot10^{-9}$
25°-30°	$(1.775\pm0.012)\cdot10^{-8}$	$(1.880\pm0.013)\cdot10^{-8}$	$(2.248\pm0.035)\cdot10^{-9}$	$(1.390\pm0.028)\cdot10^{-9}$
30°-37°	$(1.201\pm0.007)\cdot10^{-8}$	$(1.137\pm0.007)\cdot10^{-8}$	$(1.523\pm0.021)\cdot10^{-9}$	$(0.697\pm0.014)\cdot10^{-9}$

Table 2 - Current density (cm^{-2}) per source photon at the forward and lateral irradiation positions for the configuration with partial platform (case 2).

	Lateral	
	Scattered component (E < 661.6 keV)	Direct component (E = 661.6 keV)
0°-2°	$(1.842\pm0.082)\cdot10^{-6}$	$(9.482\pm0.189)\cdot10^{-6}$
2°-4°	$(1.873\pm0.048)\cdot10^{-6}$	$(9.023\pm0.106)\cdot10^{-6}$
4°-6°	$(1.805\pm0.036)\cdot10^{-6}$	$(8.311\pm0.076)\cdot10^{-6}$
6°-8°	$(1.588\pm0.028)\cdot10^{-6}$	$(7.069\pm0.060)\cdot10^{-6}$
8°-10°	$(1.474\pm0.024)\cdot10^{-6}$	$(5.843\pm0.048)\cdot10^{-6}$
	Forward	
	Pb filter 2 cm	
	Scattered component (E < 661.6 keV)	Direct component (E = 661.6 keV)
0°-5°	$(3.231\pm0.065)\cdot10^{-8}$	$(3.684\pm0.069)\cdot10^{-8}$
5°-10°	$(3.150\pm0.037)\cdot10^{-8}$	$(3.509\pm0.039)\cdot10^{-8}$
10°-15°	$(2.775\pm0.026)\cdot10^{-8}$	$(3.083\pm0.027)\cdot10^{-8}$
15°-20°	$(2.207\pm0.019)\cdot10^{-8}$	$(2.197\pm0.019)\cdot10^{-8}$
20°-25°	$(1.707\pm0.014)\cdot10^{-8}$	$(1.680\pm0.014)\cdot10^{-8}$
25°-30°	$(1.334\pm0.011)\cdot10^{-8}$	$(1.216\pm0.010)\cdot10^{-8}$
30°-37°	$(0.889\pm0.006)\cdot10^{-8}$	$(0.718\pm0.006)\cdot10^{-8}$

Table 3 - Current density (cm^{-2}) per source photon at the forward and lateral irradiation positions for the configuration with full platform (case 3).

	Lateral	
	Scattered component (E < 661.6 keV)	Direct component (E = 661.6 keV)
0°-2°	$(1.842\pm0.082)\cdot10^{-6}$	$(9.482\pm0.189)\cdot10^{-6}$
2°-4°	$(1.874\pm0.048)\cdot10^{-6}$	$(9.023\pm0.106)\cdot10^{-6}$
4°-6°	$(1.806\pm0.036)\cdot10^{-6}$	$(8.311\pm0.076)\cdot10^{-6}$
6°-8°	$(1.589\pm0.028)\cdot10^{-6}$	$(7.069\pm0.060)\cdot10^{-6}$
8°-10°	$(1.474\pm0.024)\cdot10^{-6}$	$(5.843\pm0.048)\cdot10^{-6}$
	Forward	
	Pb filter 2 cm	
	Scattered component (E < 661.6 keV)	Direct component (E = 661.6 keV)
0°-5°	$(3.657\pm0.071)\cdot10^{-8}$	$(3.697\pm0.071)\cdot10^{-8}$
5°-10°	$(3.651\pm0.048)\cdot10^{-8}$	$(3.498\pm0.046)\cdot10^{-8}$
10°-15°	$(3.328\pm0.037)\cdot10^{-8}$	$(3.185\pm0.036)\cdot10^{-8}$
15°-20°	$(3.012\pm0.029)\cdot10^{-8}$	$(2.791\pm0.028)\cdot10^{-8}$
20°-25°	$(2.522\pm0.023)\cdot10^{-8}$	$(2.416\pm0.022)\cdot10^{-8}$
25°-30°	$(2.075\pm0.018)\cdot10^{-8}$	$(1.866\pm0.017)\cdot10^{-8}$
30°-37°	$(1.450\pm0.011)\cdot10^{-8}$	$(1.172\pm0.010)\cdot10^{-8}$

Table 4 - Dose equivalent per source photon and dose equivalent rate for a 740 GBq (20 Ci) source at the accesses to the X5 facility.

	Configuration with partial platform (case 2)		Configuration with full platform (case 3)	
	Dose equivalent per source photon (Sv)	Dose equivalent rate for 740 GBq ($\mu Sv\ h^{-1}$)	Dose equivalent per source photon (Sv)	Dose equivalent rate for 740 GBq ($\mu Sv\ h^{-1}$)
Gate	$(4.935\pm0.142)\cdot10^{-22}$	1.31±0.04	$(6.478\pm0.176)\cdot10^{-22}$	1.73±0.05
PPX	$(7.110\pm0.363)\cdot10^{-22}$	1.89±0.10	$(7.148\pm0.364)\cdot10^{-22}$	1.90±0.09

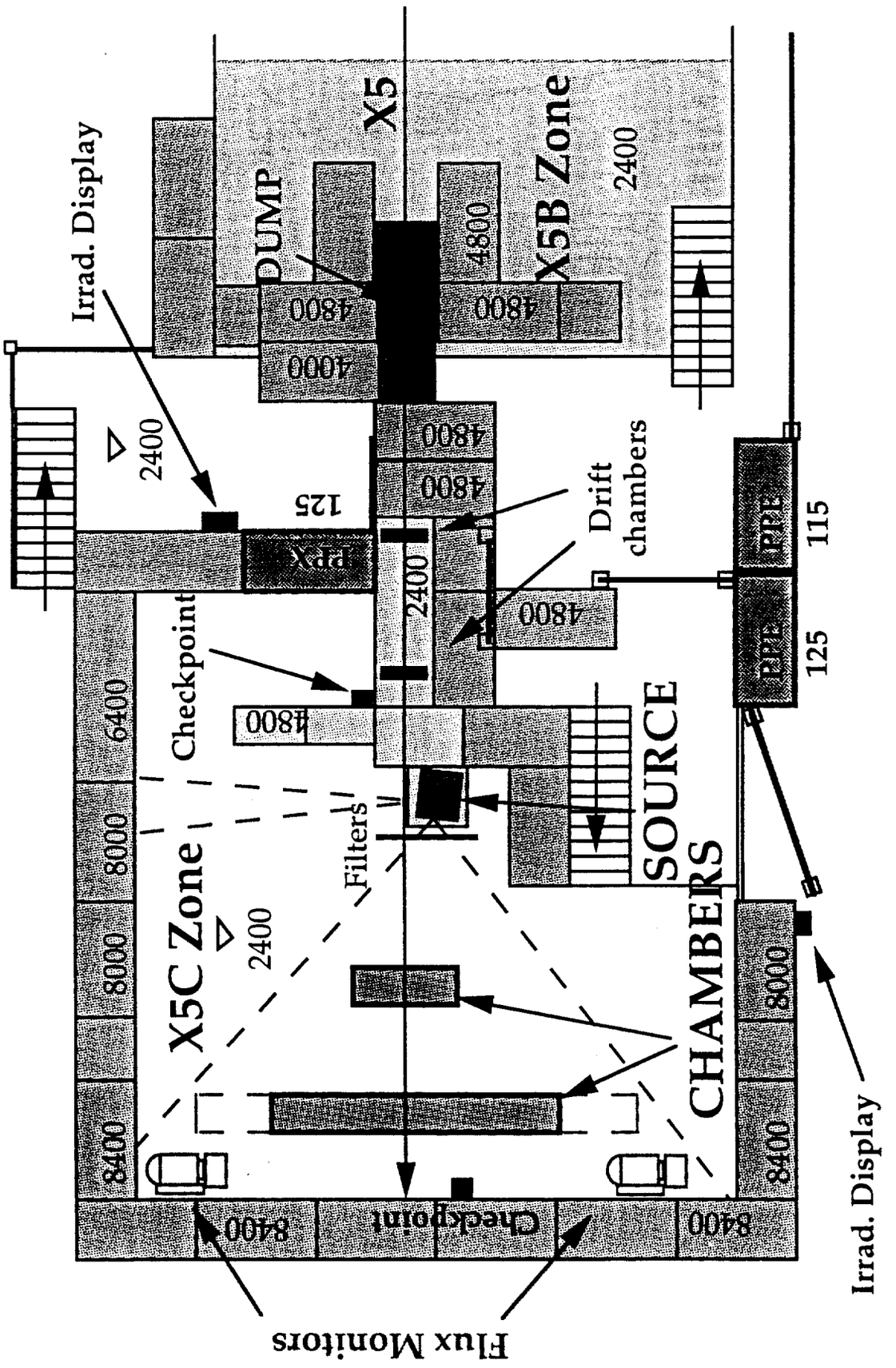

Fig. 1 Plan view of the X5C Gamma Irradiation Facility.

Fig. 2 3D sectional view of the ^{137}Cs source capsule.

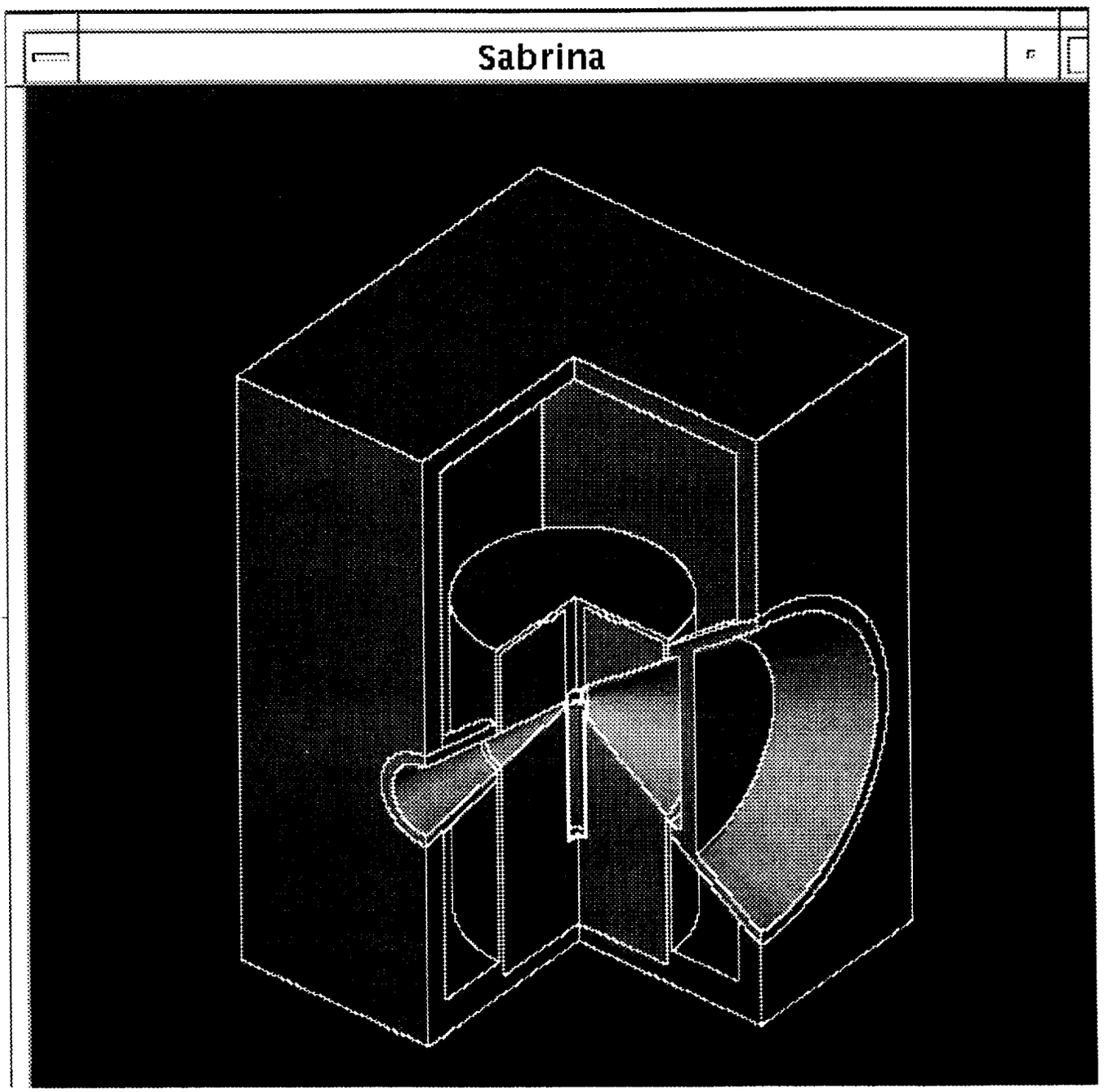

Fig. 3 3D sectional view of the source collimation system.

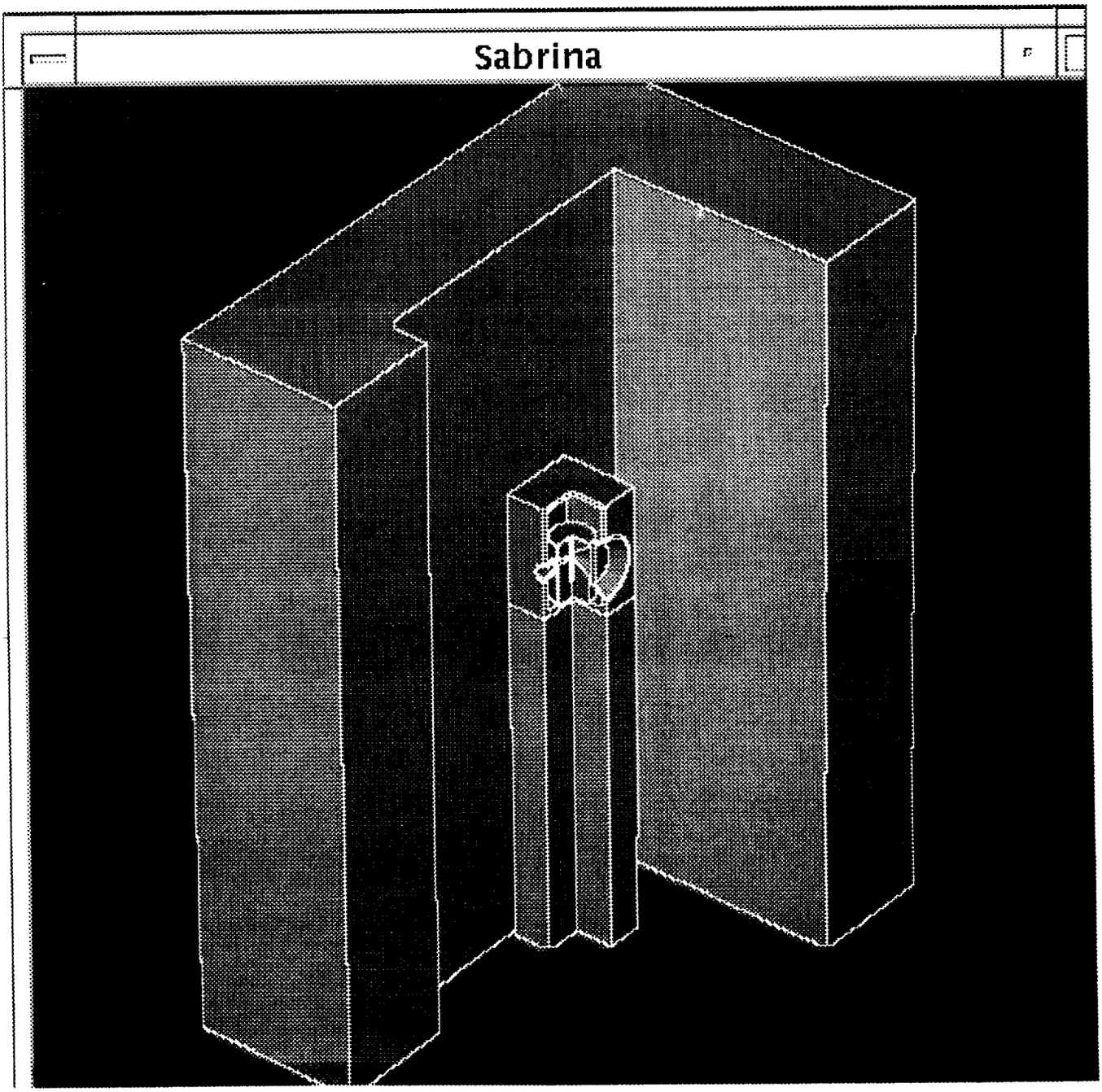

Fig. 4 3D sectional view of the source with the concrete local shield (case 1).

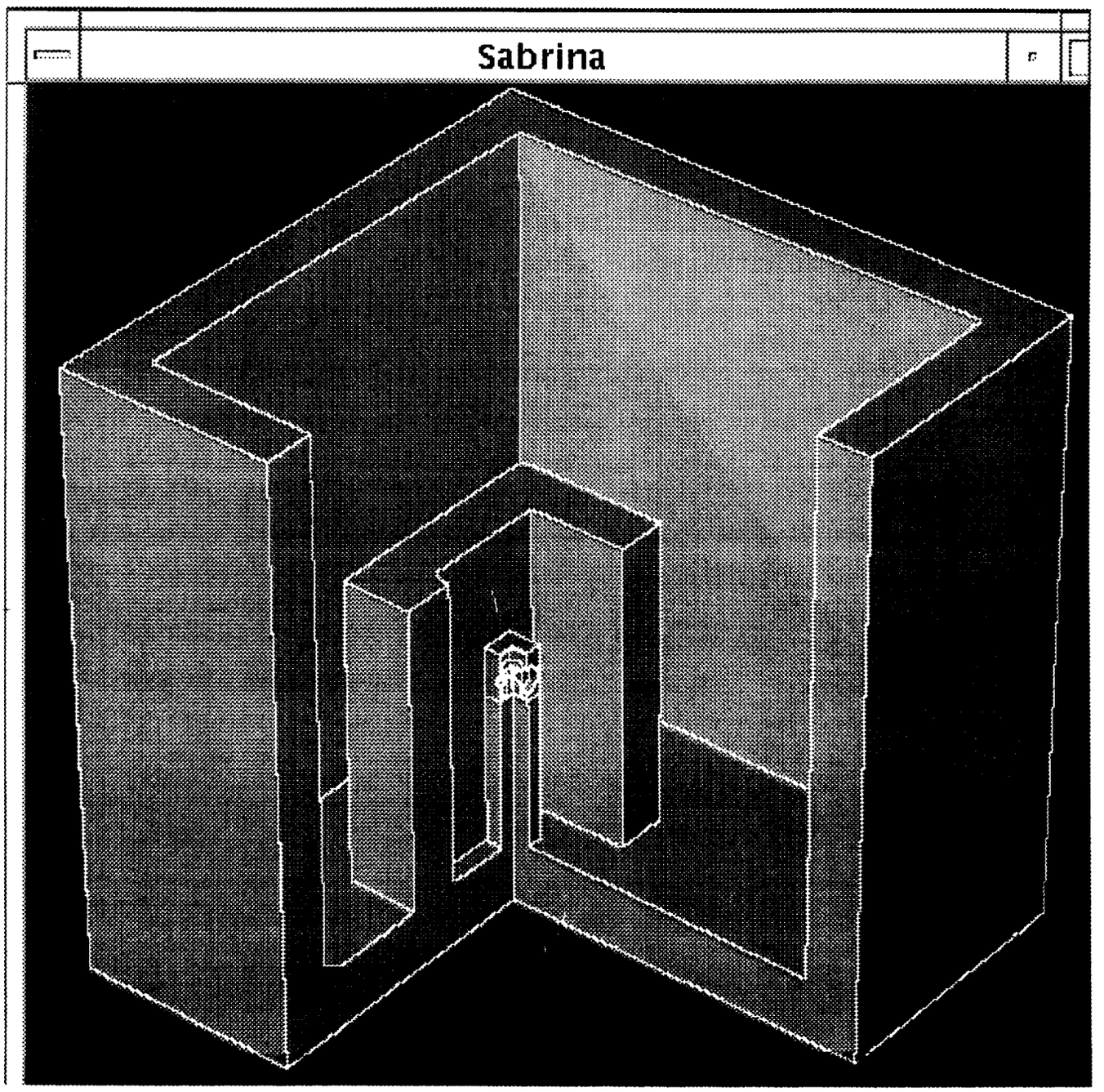

Fig. 5 3D sectional view of the facility in the configuration without platform (case 1).

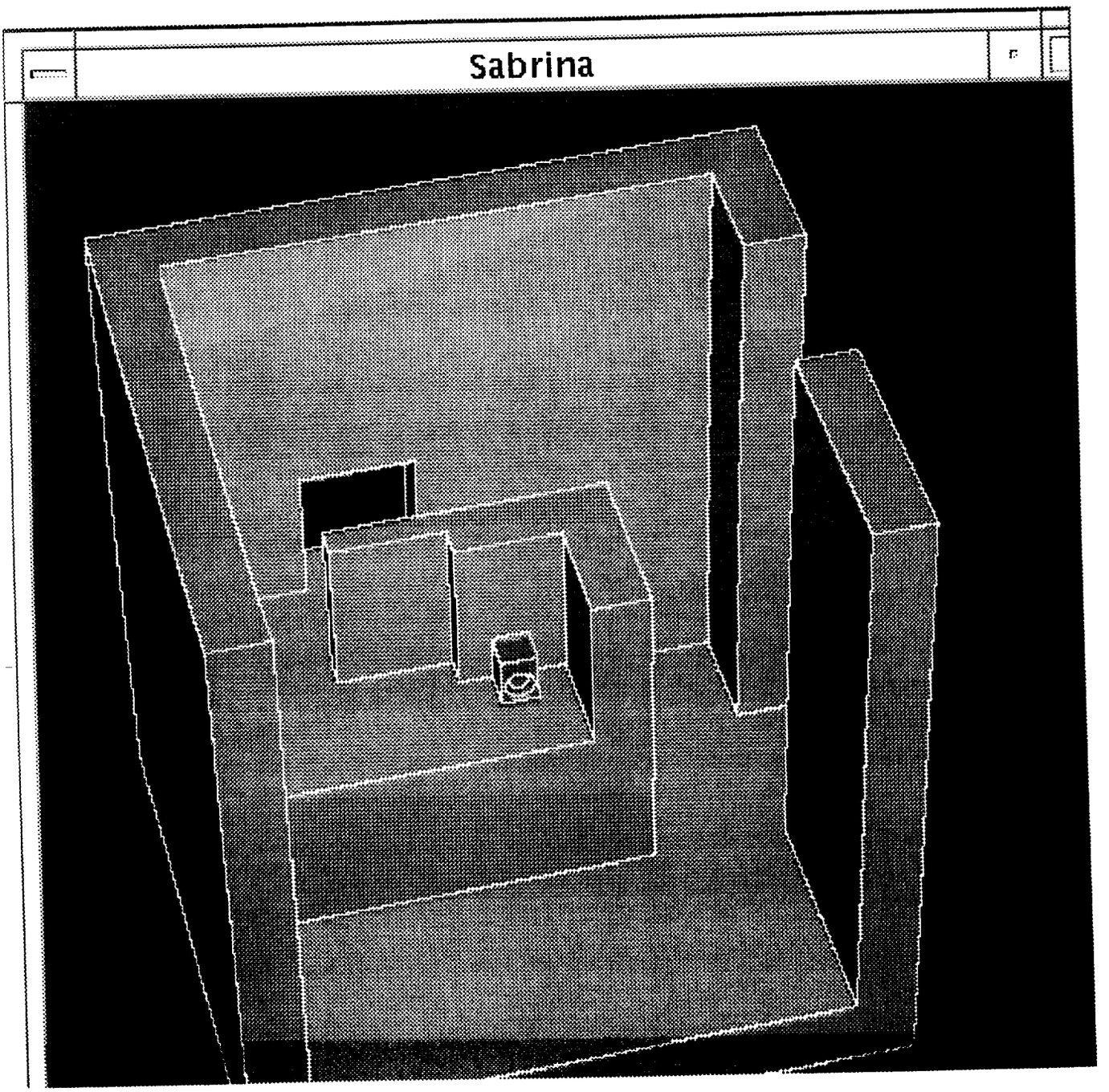

Fig. 6 3D sectional view of the facility in the configuration with partial platform (case 2). The two accesses are shown.

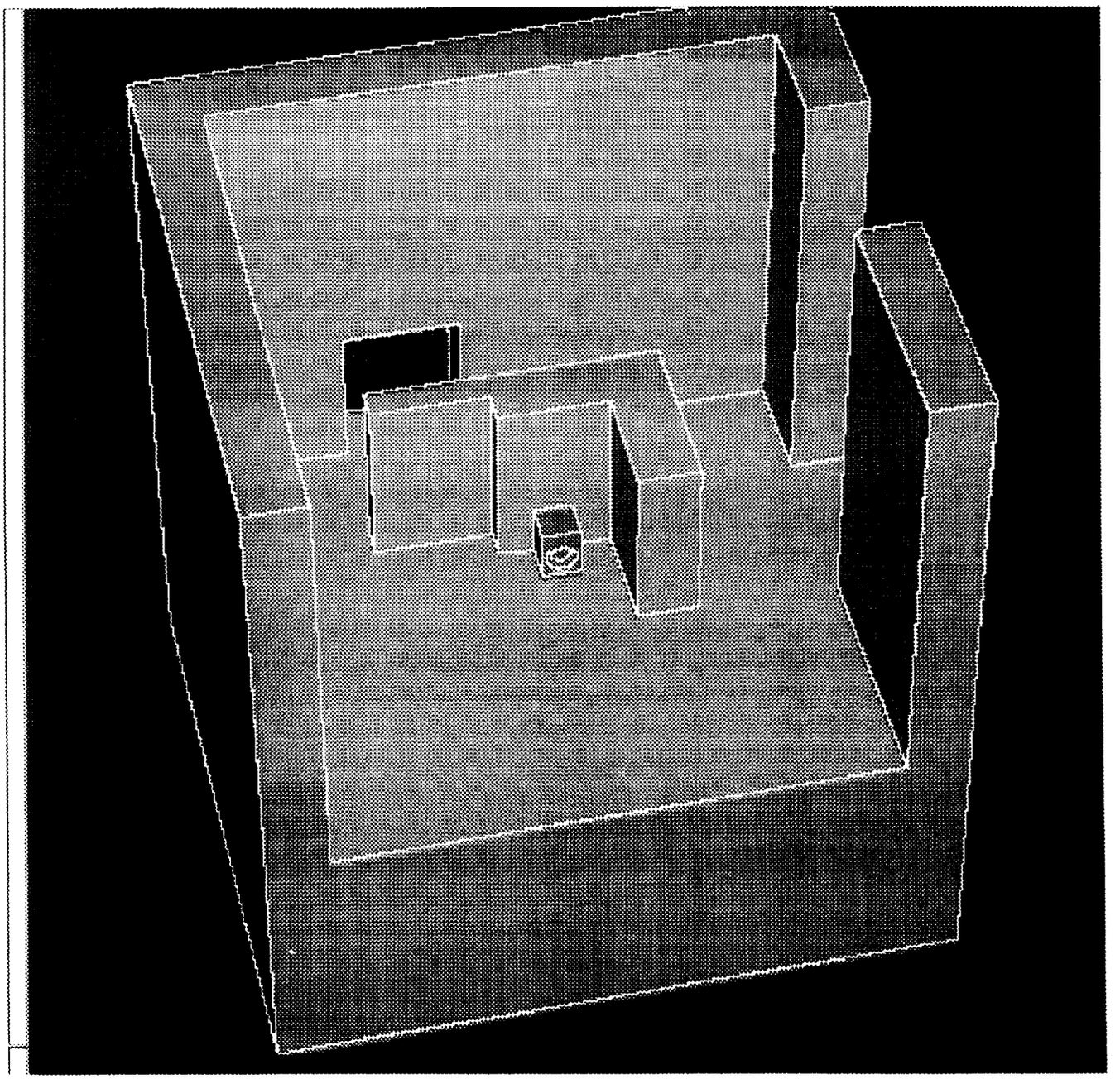

Fig. 7 3D sectional view of the facility in the configuration with full platform (case 3). The two accesses are shown.

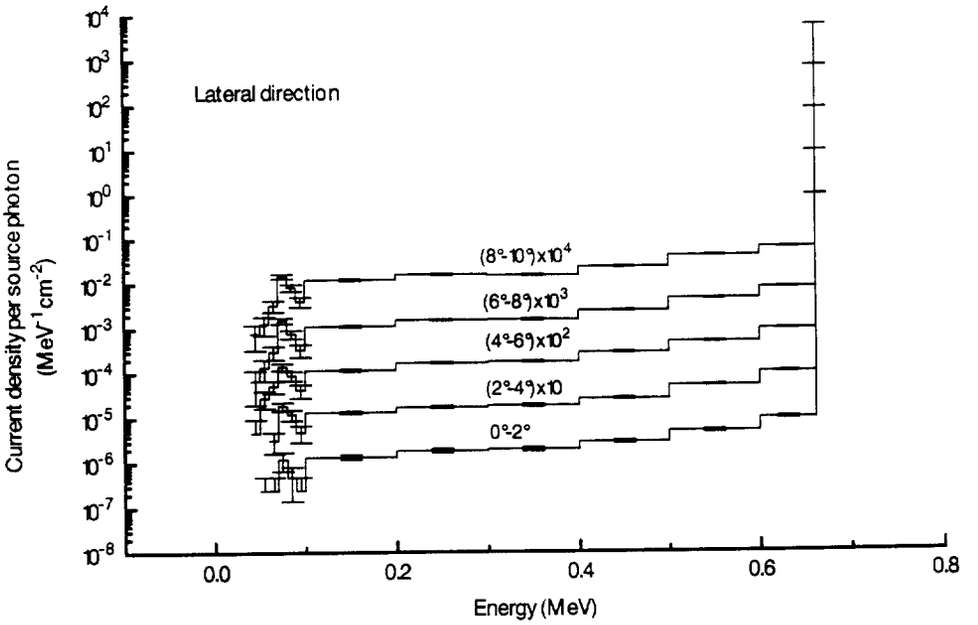

Fig. 8 Energy distribution of the current density in the lateral direction (configuration without platform, case 1).

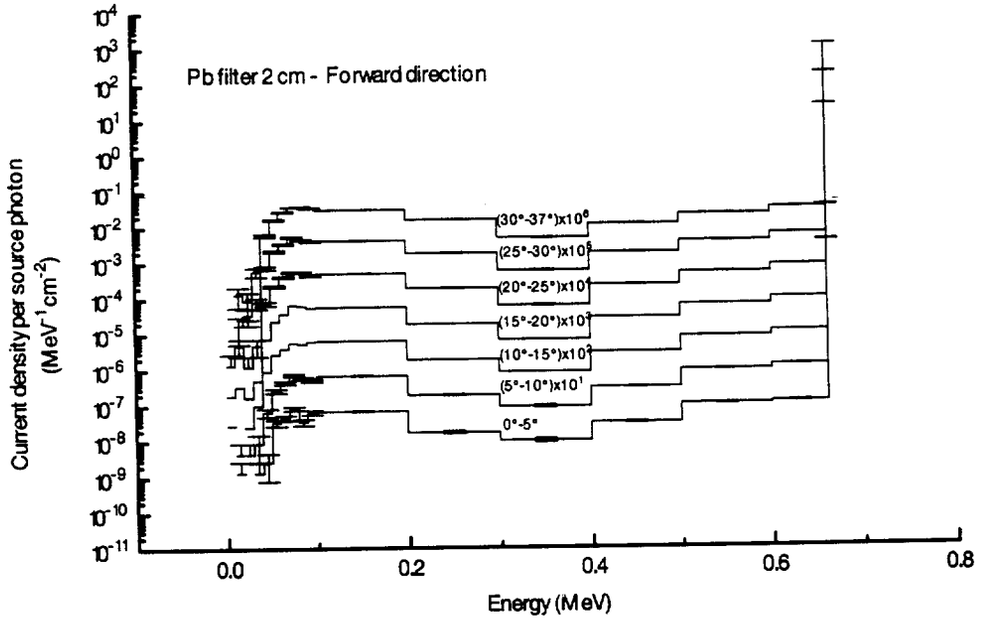

Fig. 9 Energy distribution of the current density in the forward direction (configuration without platform, case 1), with the 2 cm lead filter.

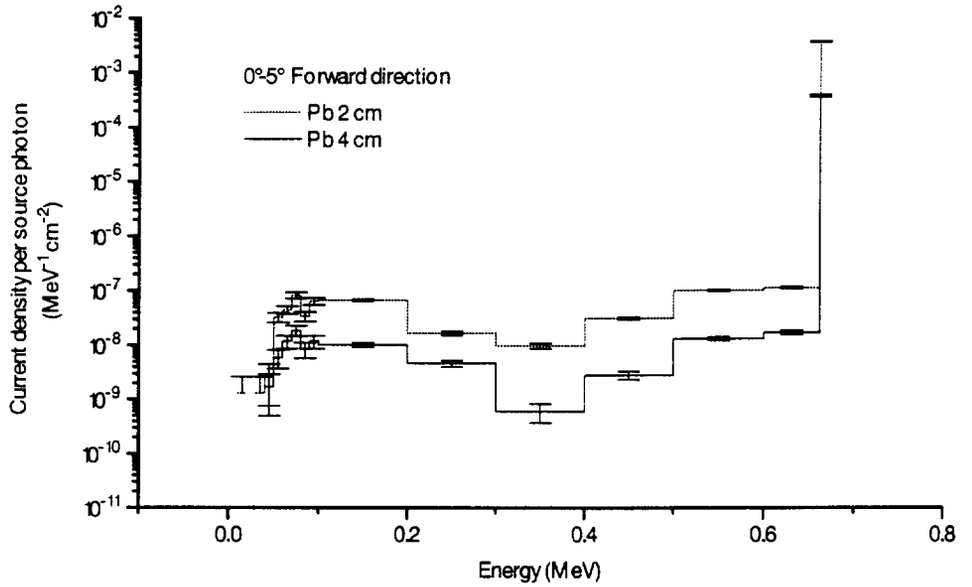

Fig. 10 Energy distribution of the current density in the forward direction in the 0°-5° angular bin with 2 cm and 4 cm lead filters (case 1).

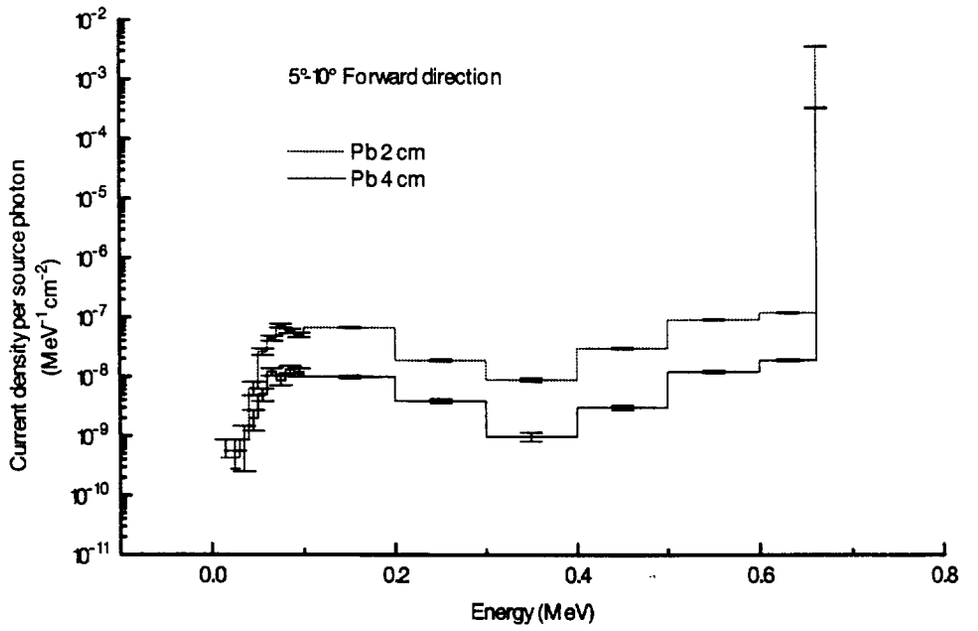

Fig. 11 Energy distribution of the current density in the forward direction in the 5°-10° angular bin with 2 cm and 4 cm lead filters (case 1).

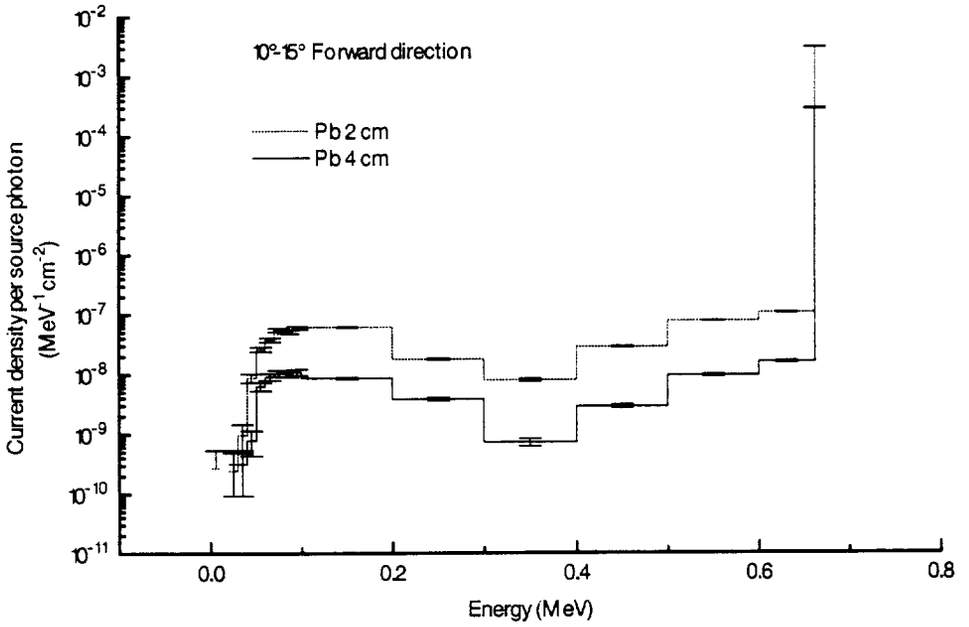

Fig. 12 Energy distribution of the current density in the forward direction in the 10°-15° angular bin with 2 cm and 4 cm lead filters (case 1).

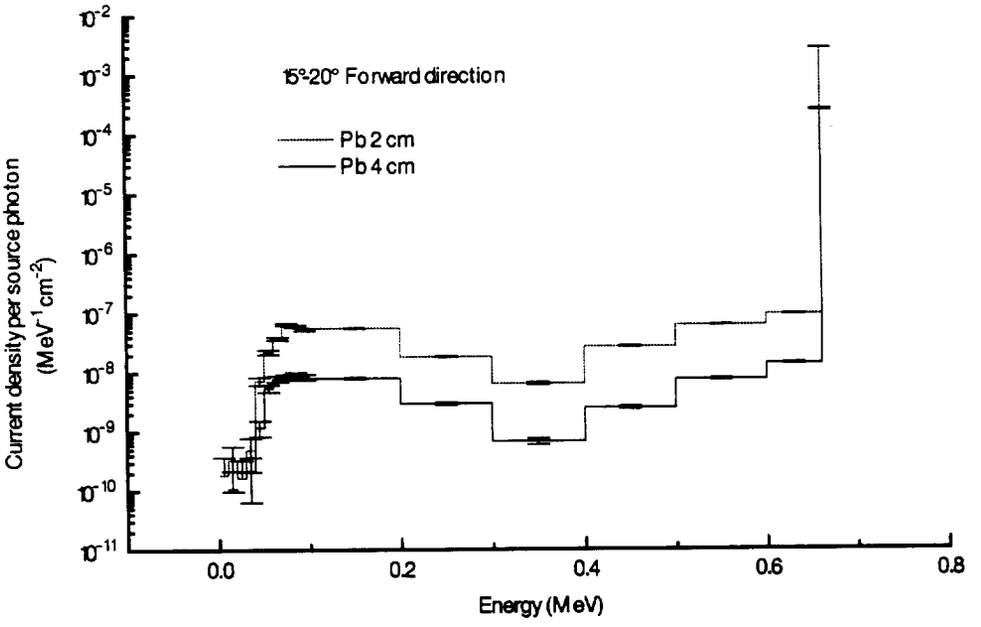

Fig. 13 Energy distribution of the current density in the forward direction in the 15°-20° angular bin with 2 cm and 4 cm lead filters (case 1).

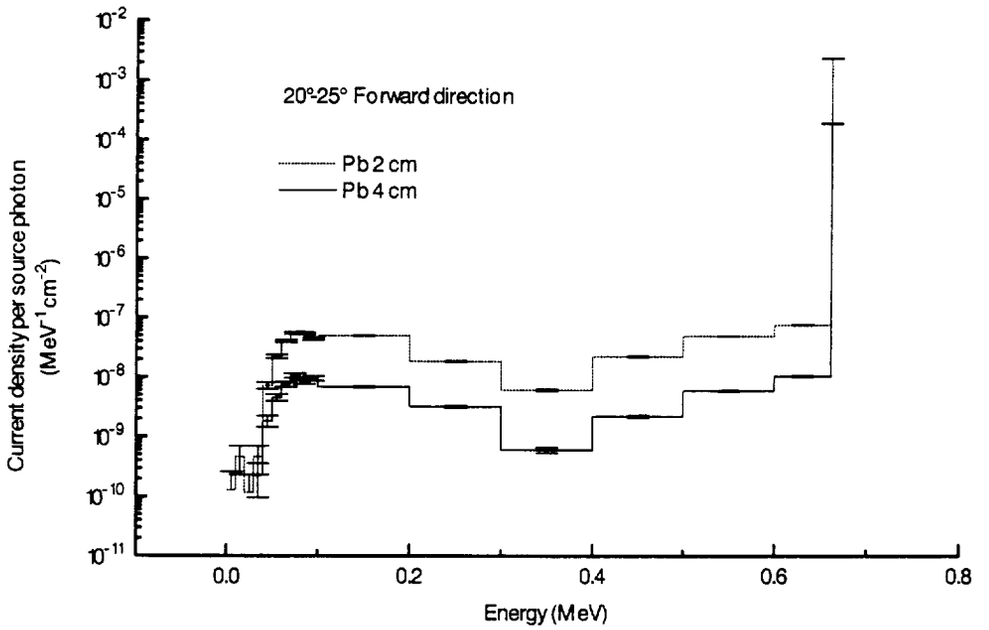

Fig. 14 Energy distribution of the current density in the forward direction in the 20°-25° angular bin with 2 cm and 4 cm lead filters (case 1).

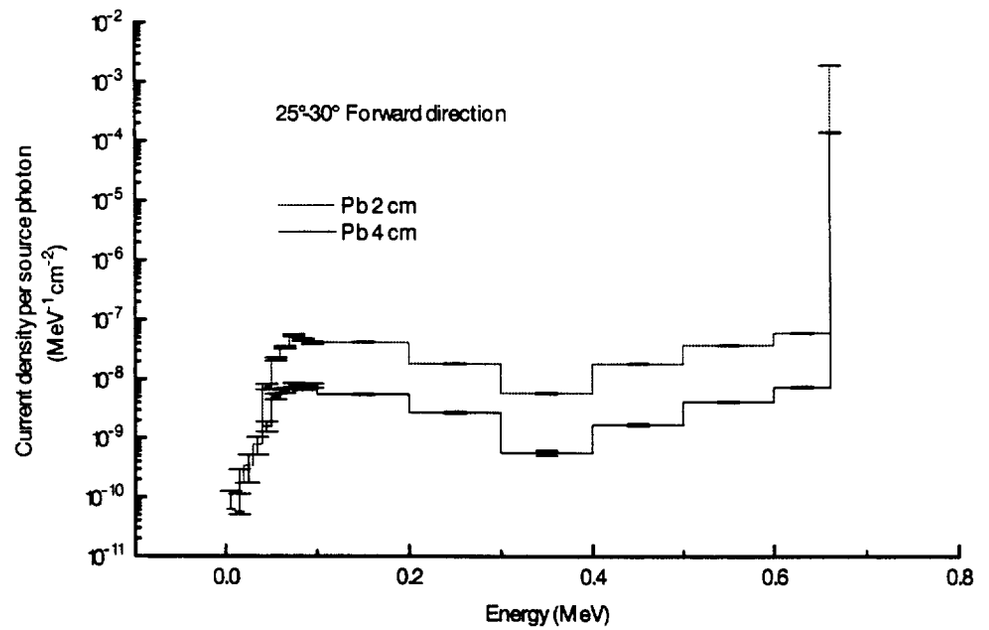

Fig. 15 Energy distribution of the current density in the forward direction in the 25°-30° angular bin with 2 cm and 4 cm lead filters (case 1).

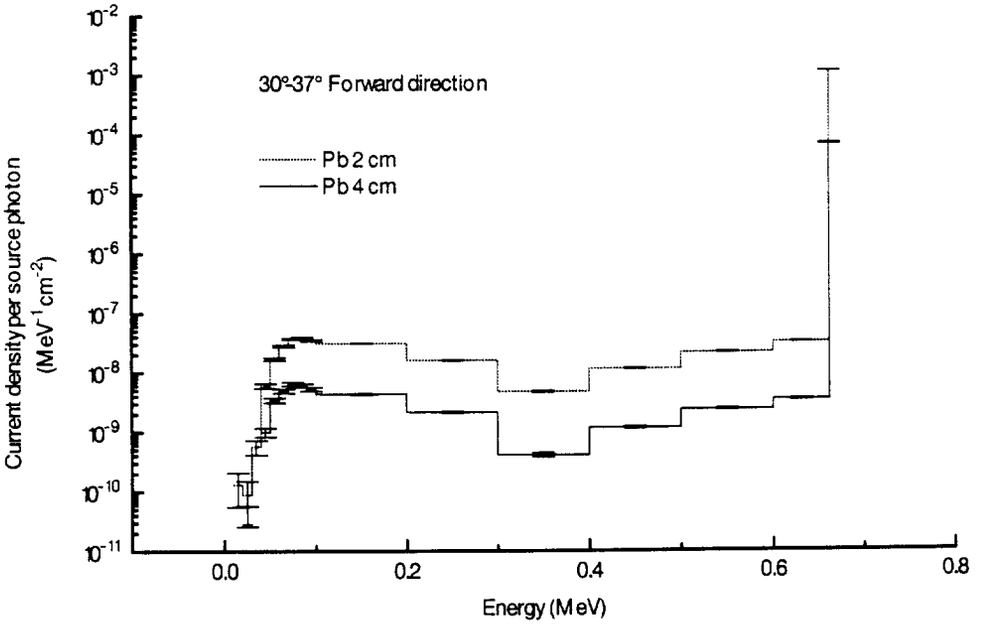

Fig. 16 Energy distribution of the current density in the forward direction in the 30°-37° angular bin with 2 cm and 4 cm lead filters (case 1).

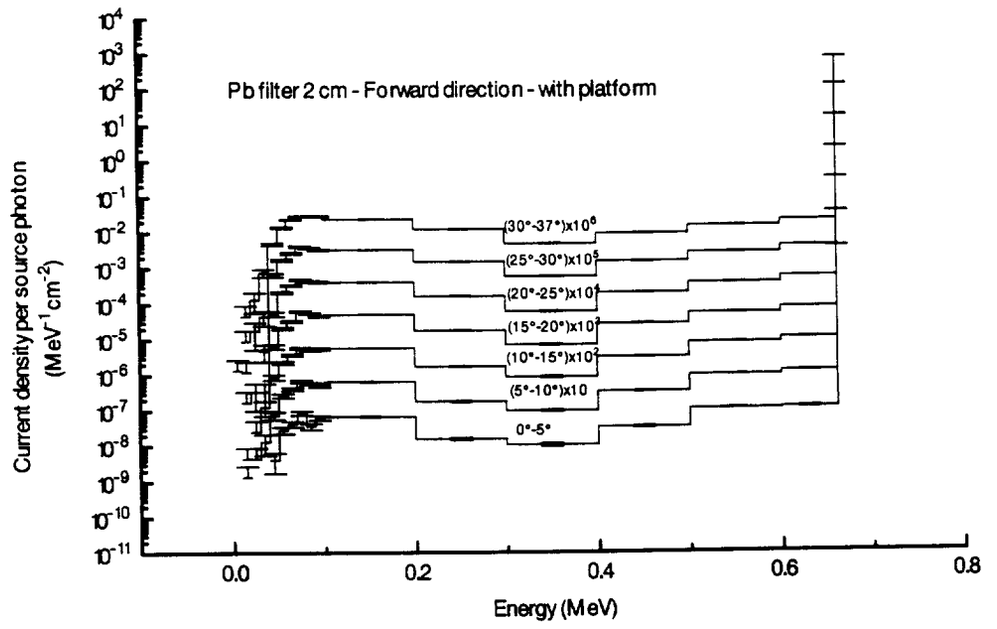

Fig. 17 Energy distribution of the current density in the forward direction (configuration with partial platform, case 2).

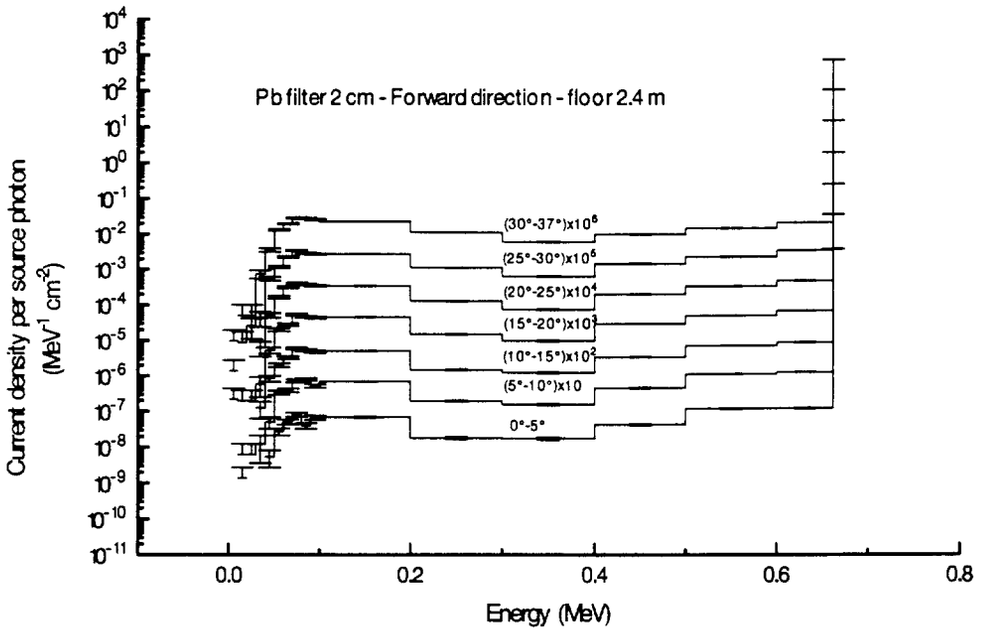

Fig. 18 Energy distribution of the current density in the forward direction (configuration with full platform, case 3).